The Design of a New Double Loop Controller For Simultaneous Adjustment of Input and Output Voltages of Single-Phase Grid-Connected Inverter

Parisa Alipour[1], Mehdi Salimi[2]

[1] Department of Engineering, Ahar Branch, Islamic Azad University, Ahar, Iran
Aigoun_1147@yahoo.com
[2] Department of Engineering, ArdabilBranch, Islamic Azad University, Ardabil, Iran
m.salimi@iauardabil.ac.ir

Abstract

  Although LCL filters are used widely in the grid connected inverters to reduce high-order harmonics, such a system increases system order and therefore sustainable design of closed-loop controller system will be complicated. Recently, the single-loop control strategy has been suggested for L or LC filter based grid-connected inverters. However, the use of single-loop control directly in LCL filter-based inverters may cause instability. In this paper, a new double-loop control strategy is presented which includes a voltage external loop and an internal loop of filter capacitor current. The external loop controls the input voltage of the grid-connected inverter. The internal loop improves system stability margin and removes the resonance of LCL filter. To obtain the transfer function of system, single-phase instantaneous power theory is used. The computer simulation has proved the feasibility of the proposed control.

Keywords: grid-connected inverters, LCL filter, double-loop control, state-space modeling

1-Introduction

   Currently power electronic converters have rapidly developed and are widely used in many fields. Distributed generation is one of the most important applications in this field in which power electronic converters are used to transmit power from renewable energy sources to global grids such as solar, wind, micro-turbine and fuel cell systems [1] to [2]. Grid-connected converters which are the key components of distributed generation are essentially voltage source converters (VSCs). Along with the increasing use of electronic equipment, the harmonic current injected into grid is growing rapidly due to polluted loads. The use of passive filters can increase power quality, but they are expensive and bulky solutions. Moreover, there is no possibility to control the produced harmonic current by different loads. Some compensation methods have been proposed to reduce current harmonic distortion and power factor correction of electrical grids. One of the most popular power compensators is an APF filter which is used as parallel or series connection with load. In this case, several different topologies can be used that include

full-bridge voltage source inverter and full-bridge current source inverter. The main goal of parallel APF system is to provide the absorbed harmonic by non-linear load in order to supply a grid with low harmonic content. Sinusoidal pulse width modulation technology is widely used in VSCs control systems in order to convert DC power to AC power. This modulation in AC will produce harmonics. Generally L, LC or LCL filters at the AC side are used to get a sinusoidal AC power. Grid-connected VSC can effectively remove high harmonic using a LCL filter. This filter provides the inherent advantages for a VSC to work in low frequency with a high-order harmonic elimination possibility. In addition, a smaller inductor is needed compared to L or LC filters [3] to [5]. But LCL filter is the third order which will increase system order, and achieving system sustainability will become more complex. Using LCL filter is more favored by grid-connected inverters. Low cost and acceptable dynamic performance are the main advantages of these filters. In this case, a smaller inductor compared to L or LC filters is needed in order to achieve the required performance. But the advantage of LCL filter in high power converters will be more prominent. Despite these features, the use of LCL filter has its own problems. For example, it is possible that the instability is created by the zero impedance in the frequency response of LCL filters. There are two main ways to reduce resonance in the grid-connected inverters: passive damping and active damping. Passive damping includes adding a passive resistance in LCL filter [6] and [7].The general approach is so

simple that the damping of system increases by adding resistance directly, however added resistance will cause additional losses. Due to simple implementation of this method, it is commonly used in industrial applications. Active damping methods are suggested to ensure system stability without power loss. A kind of control strategy is the indirect adjustment of system by inductor current control in inverter side. In [8] and [9], inverter current is used to resonance damping by the use of second order and fourth-order filter. Although the number of required sensors is low, the ultimate controller is complex. In [10] and [11], additional signals are used so that all of them are estimated on the base of certain rules. For this reason, the number of required sensors would be minimal. The disadvantage of this method is closely related to the accuracy of estimated signals that are calculated using ideal assumptions. These assumptions can cause errors and affect system stability, because the calculations depend on filter parameters. Measuring filter capacitor current or voltage for resonance damping is reported in [10] and [11]. An interesting approach is suggested in [12] so that LCL filter can be approximated into two parts from third-order system to one-order system by separating filter capacitor current. In this method, filter capacitor current should be measured too. Remarkably, the indirect adjustment of current can't remove the distortion of grid, unless forward control of grid voltage is added to it. The direct method involves direct control of grid. Additionally, a simple controller is presented in [13] to control the current. Although in [13], the system is stable, the distortion

related to grid current in the presented results is clearly visible. In [14] to [16], an additional feedback is used in order to ensure the sustainability of whole system. Moreover, in [17] to [19] there are procedures to use the third state variables of LCL filter in feedback grid. Control methods based on third variables show optimal performance and also are suitable to improve the stability of whole system. However, the cost of such a system obviously will be high due to the number of sensors. In order to obtain optimum performance in the third-order filter, filter poles should be allocated to proper points. For this purpose, some methods are suggested in [17] to [19] so that triple poles of filter seems to be adjustable ideally. Methods based on two feedback variables can assign corresponding pole. Additionally, they can have better performance with less sensors compared to methods mentioned in [17] to [19]. In [14], filter capacitor current is measured so that internal control loop is created. Internal regulator is a proper controller. Grid current is controlled by the use of external loop and a proportional resonant controller. When adjusting the controller; the problem of this method appears. In [14], selection of control parameters is discussed, but no specific method is presented to calculate parameters accurately. In this paper, a new double-loop control strategy is presented so that there is a possibility to control the input voltage and output current simultaneously. The investigations indicate that this method has not been reported in the scientific assemblies of the world.

2-System description

In Figure 1, the structure of the proposed system is shown. The main circuit can be made from an input DC source. Additionally, a single-phase full-bridge voltage source inverter and an LCL filter is used. DC source may be implemented by various sources such as photovoltaic, wind generator, storage battery, super-capacitor and etc…. However in this paper, due to the lack of reactive power exchange, the DC side will only include one capacitor. LCL filter removes high frequency switching harmonics. Grid-connected inverter controller will be discussed in the next section.

3-The design of internal current control loop

3-1-Single-phase current detection

At first, i_s and v_s are delayed a quarter of core frequency regardless of voltage harmonic components and a vertical two-phase current can be obtained as follows:

$$v_{s\alpha} = v_s = \sqrt{2}\, V_s\, \sin \omega_0 t$$
$$v_{s\beta} = -\sqrt{2}\, V_s\, \cos \omega_0 t \tag{1}$$

$$i_{s\alpha} = i_s = \sqrt{2} \sum_{n=1}^{\infty} I_{sn}\, \sin(n\omega_0 t - \theta_n)$$
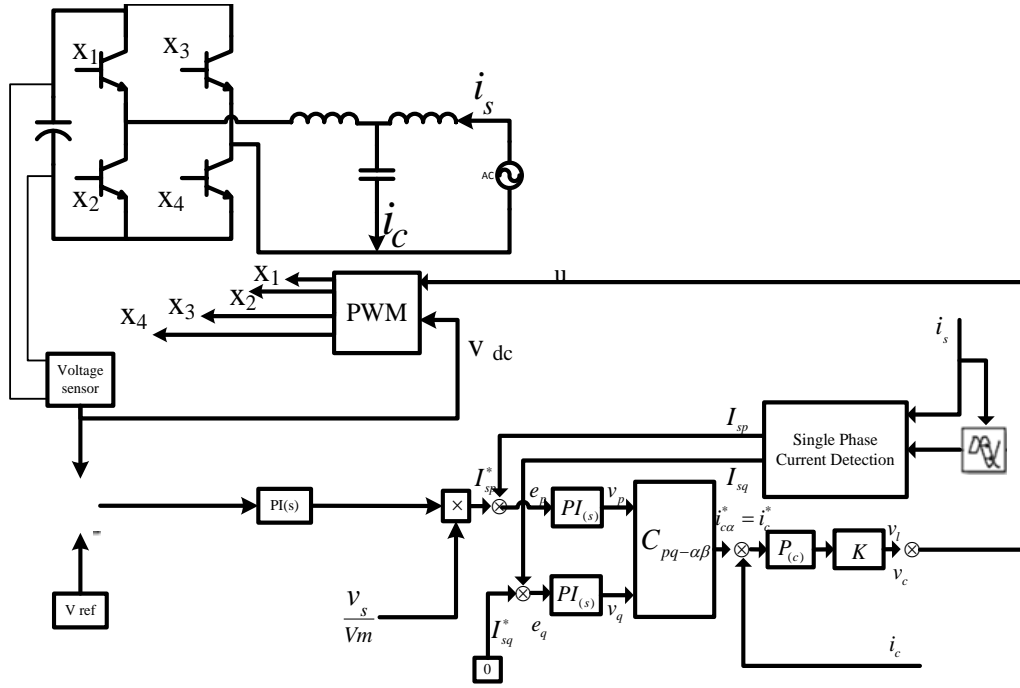$$i_{s\beta} = -\sqrt{2} \sum_{n=1}^{\infty} I_{sn}\, \cos(n\omega_0 t - \theta_n) \tag{2}$$

Fig.1. Block diagram of double-loop power control

Where V_S is the effective value of v_s and ω_0 is the frequency of main angle; I_{sn}, is the effective value of current component i_s in the angular frequency of $n\omega_0$. I_{s1} is the effective value of main current component; θn is the phase of I_s current component in the angular frequency of $n\omega_0$. According to instantaneous reactive power theory, reactive power p and active power q can be calculated using the following :

$$\begin{bmatrix} p \\ q \end{bmatrix} = \begin{bmatrix} v_{s\alpha} & v_{s\beta} \\ v_{s\beta} & -v_{s\alpha} \end{bmatrix} \begin{bmatrix} i_{s\alpha} \\ i_{s\beta} \end{bmatrix}$$

$$= \begin{bmatrix} 2V_s \sum_{n=1}^{\infty} I_{sn} \cos[(n-1)\omega_0 t - \theta_n]) \\ -2V_s \sum_{n=1}^{\infty} I_{sn} \sin[(n-1)\omega_0 t - \theta_n]) \end{bmatrix} \quad (3)$$

From Eq. 3, p and q can be decomposed into the DC components of $\bar{p}$ and $\bar{q}$. Additionally, $\tilde{p}$ and $\tilde{q}$ are AC components. $\bar{p}$ and $\bar{q}$ can be

obtained from Eq. 3 through a low-pass filter. Considering that the harmonic component (is) is low, $\tilde{p}$ and $\tilde{q}$ are small too and can be removed through LPFs.

$$\begin{bmatrix} \bar{p} \\ \bar{q} \end{bmatrix} = \begin{bmatrix} 2V_sI_{s1} \cos\theta_1 \\ 2V_sI_{s1} \sin\theta_1 \end{bmatrix} \quad (4)$$

$\bar{p}$ and $\bar{q}$ are the average values of active and reactive instantaneous power that can be related to the power exchanged between DC bus and exchanged global grid. According to Eq. 4, $\bar{p}$ and $\bar{q}$ are two times more than active and reactive power of real single-phase circuit. Here we use two capitals of Ps and Qs to indicate active and reactive power of grid-connected system:

$$\begin{bmatrix} P_s \\ Q_s \end{bmatrix} = \frac{1}{2} \begin{bmatrix} \bar{p} \\ \bar{q} \end{bmatrix} = \begin{bmatrix} V_sI_{s1} \cos\theta_1 \\ V_sI_{s1} \sin\theta_1 \end{bmatrix} \quad (5)$$

From Eq. 1 and 5,i_{s1p} instantaneous active power flow, i_{s1q}instantaneous reactive power

flow and i_{sh} harmonic current can be extracted as follows:

$$
\begin{cases}
i_{s1p} = \dfrac{v_{s\alpha}}{v^2} = \sqrt{2}I_{s1}\cos\theta_1\sin\omega_0 t \\[8pt]
i_{s1q} = \dfrac{v_{s\beta}}{v^2}\sqrt{2}I_{s1}\cos\theta_1\sin\omega_0 t \\[8pt]
i_{sh} = i_s - i_{s1p} - i_{s1q} \\[8pt]
= \sqrt{2}\displaystyle\sum_{n=3}^{\infty} I_{sn}\sin(n\omega_0 t - \theta_n)
\end{cases}
\tag{6}
$$

Total is1p and is1q component, main components of i_s are i_{s1}.

$$
i_{s1} = i_{s1p} + i_{s1q}
\tag{7}
$$

Regarding Eq. 6, it can be seen that the absolute value I_{sp}, I_{sq}, i_{s1p} respectively, and scope and are i_{s1q}

$$
\begin{bmatrix} i_{sp} \\ i_{sq} \end{bmatrix} = \begin{bmatrix} I_{sp} + \tilde{i}_{sp} \\ I_{sq} + \tilde{i}_{sq} \end{bmatrix} = C_{\alpha\beta-pq}\begin{bmatrix} i_{s\alpha} \\ i_{s\beta} \end{bmatrix}
\tag{8}
$$

$$
C_{\alpha\beta-pq} = \begin{bmatrix} \sin\omega_0 t & -\cos\omega_0 t \\ -\cos\omega_0 t & -\sin\omega_0 t \end{bmatrix}
$$

The main components of two-phase current in vertical coordinates can be obtained as follows:

$$
\begin{bmatrix} i_{s1\alpha} \\ i_{s1\beta} \end{bmatrix} = C_{pq-\alpha\beta}\begin{bmatrix} I_{sp} \\ I_{sq} \end{bmatrix}
\tag{9}
$$

Eq. 2 shows that is1αin Eq. 9 is equal to is1 in Eq. 7. The sine – cosine simultaneous with global grid can be obtained through PLL phase-locked loop from vs.

3-2-The control of grid-connected inverter

The control of grid-connected system is a double loop structure composed of power of outer loop and current inner loop. It is shown in Figure 2.

3-2-1-Power loop

Loop power adjusts power pass between DC bus and global network. A PI controller uses the references of P_S and Q_S to adjust the active and reactive power. For simple implementation, power loop can be converted to current loop of network side. Also, it can be stated that the adjustments of P_S and Q_S are equivalent with I_{sp} and I_{sq} currents of grid active and active power. In section 3, the way to obtain I_{sp} and I_{sq} is analyzed I_{sp} and I_{sq} values are DC and PI controller that can guarantee zero steady state error. Precise adjustment of grid-connected power has been proved and power factor can be controlled too. In Figure 1, active and reactive power flow errors e_{sp} and e_{sq} are controlled by PI_S and inner loop of current is obtained through transformation matrix Cpq –αβ and ic* references. Power loop with details listed in Figure (1) is consistent with power external loop in Figure (2). Gs(s) states the transform function of PI_S as:

$$
G_S(s) = K_{sp} + \frac{Ksi}{s}
\tag{10}
$$

$$
\begin{cases}
I_{sp}^* = \sqrt{2}P_s^*/V_s \\
I_{sq}^* = \sqrt{2}Q_s^*/V_s
\end{cases}
\tag{11}
$$

From Eq. (9) and Figure (2a), the following equation can be derived:

$$
\begin{aligned}
\begin{bmatrix} e_{sp} \\ e_{sq} \end{bmatrix} &= \begin{bmatrix} I_{sp}^* \\ I_{sq}^* \end{bmatrix} - \begin{bmatrix} I_{sp} \\ I_{sq} \end{bmatrix} \\[6pt]
&= C_{\alpha\beta-pq}\begin{bmatrix} i_{s\alpha}^* \\ i_{s\beta}^* \end{bmatrix} - C_{\alpha\beta-pq}\begin{bmatrix} i_{s\alpha} \\ i_{s\beta} \end{bmatrix} \\[6pt]
&= C_{\alpha\beta-pq}\begin{bmatrix} i_{s\alpha}^* - i_{s\alpha} \\ i_{s\beta}^* - i_{s\beta} \end{bmatrix} = C_{\alpha\beta-pq}\begin{bmatrix} e_{s\alpha} \\ e_{s\beta} \end{bmatrix}
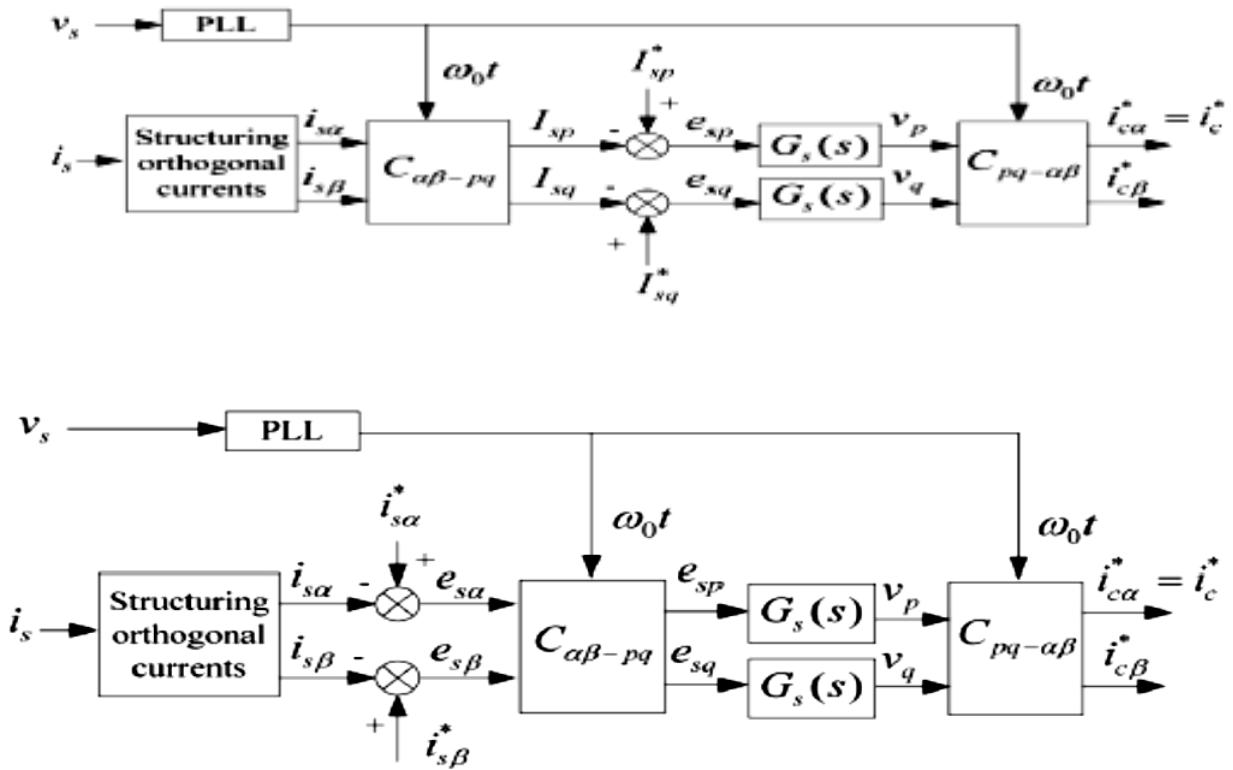\end{aligned}
\tag{12}
$$

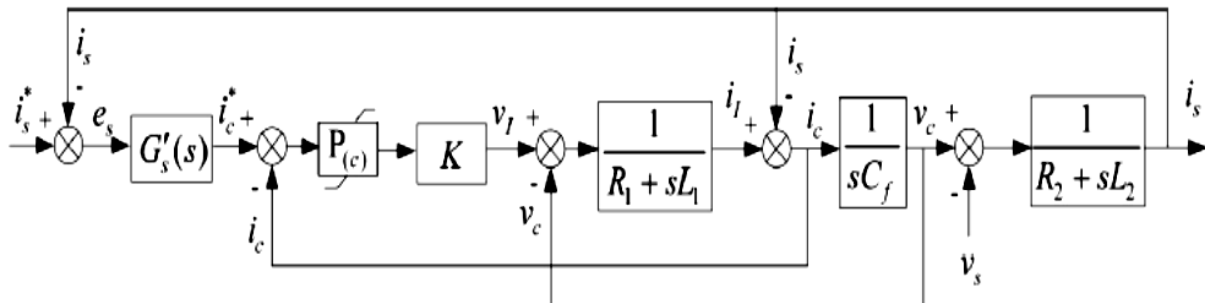**Fig.2.**Double-loop transfer function controller A) Initial power ring B) equivalent power loop

Fig.3. Diagram structure of equivalent double-loop current control

From Eq. (12) and Figure (2b), the time domain expression of Eq. 12 can be written as follows:

$$\begin{cases} e_{s\alpha}(t) = e_{s\alpha}(t) \sin \omega_0 t - e_{s\beta}(t) \cos \omega_0 t \\ e_{s\beta}(t) = -e_{s\alpha}(t) \cos \omega_0 t - e_{s\beta}(t) \sin \omega_0 t \end{cases} \tag{13}$$

30

The time domain expression of PI$_S$ controller with the outputs of V$_P$ and V$_q$ in Figure (2b) can be stated as follows:

$$\begin{cases} v_p(t) = e_{sp}(t) * g_s(t) \\ v_q(t) = e_{sq}(t) * g_s(t) \end{cases} \tag{14}$$

Where *refers to the complexity of multiplication and g$_s$(t) indicates time domain function of G$_s$(s). i$^*_{c\alpha}$ and i$^*_{c\beta}$ the reference currents of internal loop can give V$_P$ and V$_q$ through C$_{pq-\alpha\beta}$

Time domain term of i$^*_{c\alpha}$ and i$^*_{c\beta}$ after coming out from Laplace transform function (Eq.15) can be written as Eq.16. $\mathcal{L}$ sign is referring to the Laplace operator. Clearly, it turns out that the whole complexity of the signal in the time domain is equal to two signals in the frequency domain. By substituting Eq. 13 in Eq. 14 and then taking the time domain Laplace, V$_P$ and V$_q$ can be expressed as Eq.17.

$$\begin{cases} i^*_{c\alpha}(t) = v_p(t)\sin\omega_0 t - v_q(t)\cos\omega_0 t \\ i^*_{c\beta}(t) = -v_q(t)\cos\omega_0 t - v_q(t)\sin\omega_0 t \end{cases} \tag{15}$$

$$\begin{cases} I^*_{c\alpha}(s) = \mathcal{L}[v_p(t)\sin\omega_0 t] - \mathcal{L}[v_q(t)\cos\omega_0 t] \\ I^*_{c\beta}(s) = -\mathcal{L}[v_q(t)\cos\omega_0 t] - \mathcal{L}[v_q(t)\sin\omega_0 t] \end{cases} \tag{16}$$

$$\begin{cases} V_p(s) = \mathcal{L}[e_{s\alpha}(t)\sin\omega_0 t - e_{s\beta}(t)\cos\omega_0 t]Gs(s) \\ V_q(s) = \mathcal{L}[-e_{s\alpha}(t)\cos\omega_0 t - e_{s\beta}(t)\sin\omega_0 t]Gs(s) \end{cases} \tag{17}$$

By substituting 17 in 16 and similar to 18 and 19, according to the convolution in the frequency domain characteristics, the following equations can be extracted:

$$\begin{cases} \mathcal{L}[f(t)\sin\omega_0 t] = \dfrac{j}{2}[F(s+j\omega_0) - F(s-j\omega_0)] \\ \mathcal{L}[f(t)\cos\omega_0 t] = \dfrac{1}{2}[F(s+j\omega_0) + F(s-j\omega_0)] \end{cases} \tag{18}$$

$$\begin{cases} I^*_{c\alpha}(s) = \dfrac{1}{2}E_{s\alpha}(s)[G_s(s+j\omega_0) + G_s(s-j\omega_0)] - \dfrac{j}{2}E_{s\beta}(s)[G_s(s+j\omega_0) - G_s(s-j\omega_0)] \\ I^*_{c\beta}(s) = \dfrac{j}{2}E_{s\alpha}(s)[G_s(s+j\omega_0) - G_s(s-j\omega_0)] + \dfrac{1}{2}E_{s\beta}(s)[G_s(s+j\omega_0) + G_s(s-j\omega_0)] \end{cases} \tag{19}$$

By substituting Eq. 10 in Eq. 19, the following equation can be obtained:

$$\begin{bmatrix} I^*_{c\alpha}(s) \\ I^*_{c\beta}(s) \end{bmatrix} = \begin{bmatrix} K_{sp} + \dfrac{K_{si}s}{s^2+\omega_0^2} & -\dfrac{k_{si}\omega_0}{s^2+\omega_0^2} \\ \dfrac{k_{si}\omega_0}{s^2+\omega_0^2} & K_{sp} + \dfrac{K_{si}s}{s^2+\omega_0^2} \end{bmatrix} \begin{bmatrix} E_{s\alpha}(s) \\ E_{s\alpha}(s) \end{bmatrix} \tag{20}$$

3-2-2-Current loop

There are a number of variables that behave as control variables in the inner loop, such as i_1 and v_1 (referring to the voltage across L_1, R_1), i_c, v_c, However, only i_c can be considered as a control variable for the damping resonance with the filter LCL. Here the inner loop uses a proportional controller P, because the steady state error of the inner loop has no effect on regulating accuracy of the system.

3-2-3-Design of internal control and stability analysis

We assume that Vdc is constant and the switching frequency is high enough, VSC can be entitled proportional element K that is equal to the output voltage V_1 in the inner loop. In accordance with the Eq. 20, the double-loop control in Figure 1 can control the flow of two-loop structure shown in Figure 3 as an equivalent amount. Here $E_{s\beta}$ (s) is assumed to be zero transfer function controller. PI, $G_S(s)$ of $G_S(s)$ have been laid and this is written in Eq.21. The frequency domain in Figure 3 can be extracted and expressed in Eq.22. Open-loop and closed-

loop transfer function of the network is able to arrange the Eq.23 and Eq.24 extracted as the grid voltage Vs that can be used as a disturbance in the relationship and Vs (s), is initialized to zero.

$$\acute{G}_s(s) = K_{sp} + \frac{K_{si}s}{s^2 + \omega_0^2} \tag{21}$$

The parameters of the components of Figure 1 are listed in Table 1. In Figure 4 a root locus is plotted in MATLAB. Poles of the closed-loop are shown. In Figure (6) k_{SP} increases from 0.1 to 0.5 can improve system stability, because the pole can move around the imaginary axis. When k_{SP} 2, a pair of poles on the imaginary axis, is in right plane and the system can be unstable, with an increase in k_{si} and k_{SP} for unknown stability, the larger outer loop integral k_{si}, steady state error of the system that can less likely increase the proportion of inner ring k_{SP} can increase the open-loop system. Amplitude and phase margins are created by 10dB and 73 degrees when k_{cp} on 0.2. If k_{cp} is 1, the phase margin of 10 dB and 39 degree phase margin. Reduce k_{cp} increases the resonance damping of system also k_{cp} and k_{si} and k_{sp} 1 are respectively 0.5 and 100.

According to the Eqations 18, 19, 20 and 21 the function below will be extracted:

$$\begin{aligned}
E_s(s)&\acute{G}_s(s)K_{cp}K \\
&= \left[L_1C_fS^2 + \left(R_1 + K_{cp}\right)C_f(s) + 1\right]V_s(s) \\
&+ (a_3s^3 + a_2s^2 + a_1s + a_0s^0)I_s(s)
\end{aligned} \tag{22}$$

In this equation we have:

$$a_3 = L_1L_2C_f \,, a_2 = \left(R_1 + K_{cp}K\right)L_2C_f + R_2L_1C_f \,, \tag{23}$$

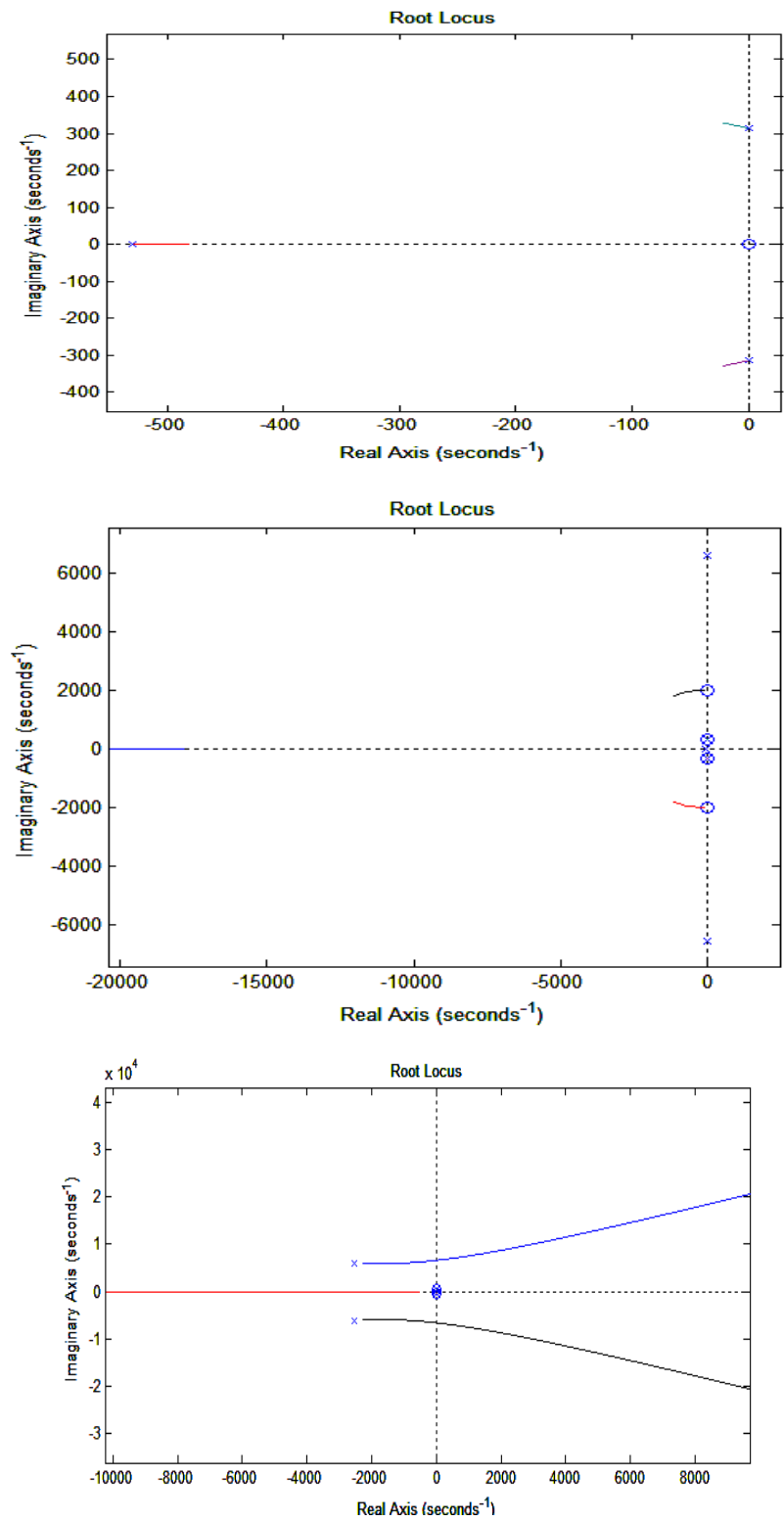$$a_1 = L_1 + L_2 + R_1R_2C_f + R_2K_{cp}KC_f \,, a_0 = R_1 + R_2$$

Fig. 4. Closed loop transfer function root locus of control $k_{cp}=20$, $k_{si}=0.2$, $k_{sp}=0.15$

4-Outer Loop Voltage

In a control system, stability condition requires that the states of the system must always reach to a stable equilibrium point. Low-frequency dynamics of APF system has been expressed by nonlinear equations.

$$\frac{d < i_i >}{dt} = k_i(v_c^* - < v_c >) \tag{24}$$

$$\begin{aligned} &\frac{d < i_L >}{dt} \\ &= \frac{1}{L}\Big(< v_S > - < i_s - i_o \\ &> . r_L \\ &- \frac{< v_c > . < i_s >}{k_p(v_c^* - < v_c >) + < i_i >)} \Big) \end{aligned} \tag{25}$$

$$\begin{aligned} &\frac{d < v_c >}{dt} \\ &= \frac{1}{C}\Big(\frac{< i_s - i_o > . < i_s >}{k_p(v_c^* - < v_c >) + < i_i >)}\Big) \end{aligned} \tag{26}$$

In this section, a stability using small signal model is investigated. APF system has shown that a small signal model can only include a dynamic voltage [20]. In this section the nonlinear model in small signal model is used in order to complete the design requirements. Nonlinear model Variables' equations in general consist of the dc and ac components. Only the ac frequency component with information has been used in design process.

These components can be non-linear model on the half-period average of the extracted network [21] and [22]. Therefore, all variables in the system can be fixed with an average value, in addition to small signal changes shown. It is noteworthy that small signal variations due to the average of the low frequency waveforms are non-sinusoidal. Averaged variables can be shown as follows:

$$\bar{\imath}_L = I_L + \hat{\imath}_L(t) \tag{27}$$

$$\bar{v}_c = V_c + \hat{v}_c(t) \tag{28}$$

$$\bar{\imath}_i = I_i + \hat{\imath}_i(t) \tag{29}$$

$$\bar{v}_s = V_s + \hat{v}_s(t) \tag{30}$$

$$\bar{\imath}_s = I_s + \hat{\imath}_s(t) \tag{31}$$

$$\bar{\imath}_o = I_o + \hat{\imath}_o(t) \tag{32}$$

$$\bar{\imath}_{o1} = I_{o1} + \hat{\imath}_{o1}(t) \tag{33}$$

It is noteworthy that two currents in (32) and (33) are marked. First i_o, the current absorbed by the non-linear load. Second harmonic component is $i_o . <I_s>$ achieved in 17 states. It is noteworthy that the average result is a sinusoidal signal and a signal with high harmonic content $<i_s - i_o>$. Only the first harmonic component is equal to zero. By substituting equations (22) - (28) (15) - (17) and the average of the half period of the ac and static network model comes with different variables:

$$\begin{aligned} &\frac{d\big(I_s + \hat{\imath}_s(t)\big)}{dt}L - \frac{d\big(I_o + \hat{\imath}_o(t)\big)}{dt}L \\ &= V_s + \hat{v}_s(t) - r_L\big(I_s + \hat{\imath}_s(t) - I_o - \hat{\imath}_o(t)\big) \\ &- \frac{\big(V_c - \hat{v}_c(t)\big)\big(I_s + \hat{\imath}_s(t)\big)}{k_p\big(v_c^* - V_c - \hat{v}_c(t)\big) + I_i + \hat{\imath}_i(t)} \end{aligned} \tag{34}$$

$$\frac{d\big(V_c + \hat{v}_c(t)\big)}{dt} = \frac{\pi^2}{8c}\left(\frac{\big(I_s + \hat{\imath}_s(t)\big)\big(I_s + \hat{\imath}_s(t) - I_{o1} - \hat{\imath}_{o1}(t)\big)}{k_p\big(v_c^* - V_c - \hat{v}_c(t)\big) + I_i + \hat{\imath}_i(t)}\right) \tag{35}$$

$$\frac{d\big(I_i + \hat{\imath}_i(t)\big)}{dt} = k_i\big(v_c^* - V_c - \hat{v}_c(t)\big) \tag{36}$$

Just using static values, relationship under steady-state is derived

$$I_i = \frac{V_c I_s}{V_s + r_L(I_o - I_s)}$$
$$= \frac{v_c^* i_{o1.rms}}{v_{s,rms} + r_L(i_{o,rms} - i_{o1,rms})} \tag{37}$$

$$I_s = I_{o1} = \frac{2\sqrt{2}}{\pi} i_{o1,rms} \tag{38}$$

$$V_c = v_c^* \tag{39}$$

Here $v_{s,\,rms}$ and $I_{o1,\,rms}$ are rms values of harmonic voltage and load current. See Table 4-1.

By substituting equations (37) - (39) to (34) - (36) and ignoring the ac component of the second order, V_c variable closed loop of small-signal model is obtained. In Laplace, domain model can be expressed as follows:

$$(s^3 + a_2 s^2 + a_1 s + a_0)\hat{v}_c(s) = f(\hat{v}_s(s), \hat{\imath}_o(s), \hat{\imath}_{o1}(s)) \tag{40}$$

$$a_2 = \frac{v_c^* + I_i \cdot r_L}{I_i \cdot L} \tag{41}$$

$$a_1 = \frac{i_{o1,rms}}{CLI_i^2}\big(i_{o1,rms} + k_p(v_{s,rms} + r_L(i_{o,rms} - i_{o1,rms}))\big) \tag{42}$$

$$a_0 = \frac{k_i i_{o1,rms}}{CLI_i^2}\big(v_{s,rms} + r_L(i_{o,rms} - i_{o1,rms})\big) \tag{43}$$

Considering the linear model obtained in the equation (40), stability analysis using sustainability criteria Ruth-Horvitz can be done.

$$k_p > -\frac{i_{o1,rms}}{v_{s,rms} + r_L(i_{o,rms} - i_{o1,rms})} \tag{44}$$

$$0 < k_i < \frac{(v_c^* + I_i \cdot r_L)(i_{o,rms} + k_p(v_{s,rms} + r_L(i_{o,rms} - i_{o1,rms})))}{I_i \cdot L(v_{s,rms} + r_L(i_{o,rms} - i_{o1,rms}))} \tag{45}$$

5- Simulation Results

In Figures 5 a , b, for a step change in the dynamic response of the proposed controller shows the reactive power. The simulation results in cases where the reference value P*S and Q*S=1 and 500 kW of active power and reactive are shown both to be connected to the network completely, reference values and can be seen in the steady state tracking. Coupling between the active and non-active on this bug does not affect the system transient response. Flow regulator can be enabled and disabled according to the corresponding network. Active power and reactive of grid connected inverter are shown in Figure 5(a). Simulated system based on fig (6) is given below.

We see that the dynamic response of the current waveform at the time of 0.2 seconds in the network 5 (b) is acceptable. In Fig. 7, simulation results related to the national grid voltage waveform were shown and the current network is represented in Fig.8. In the diagram, the open loop transfer function for proportional gain inner loop is shown.
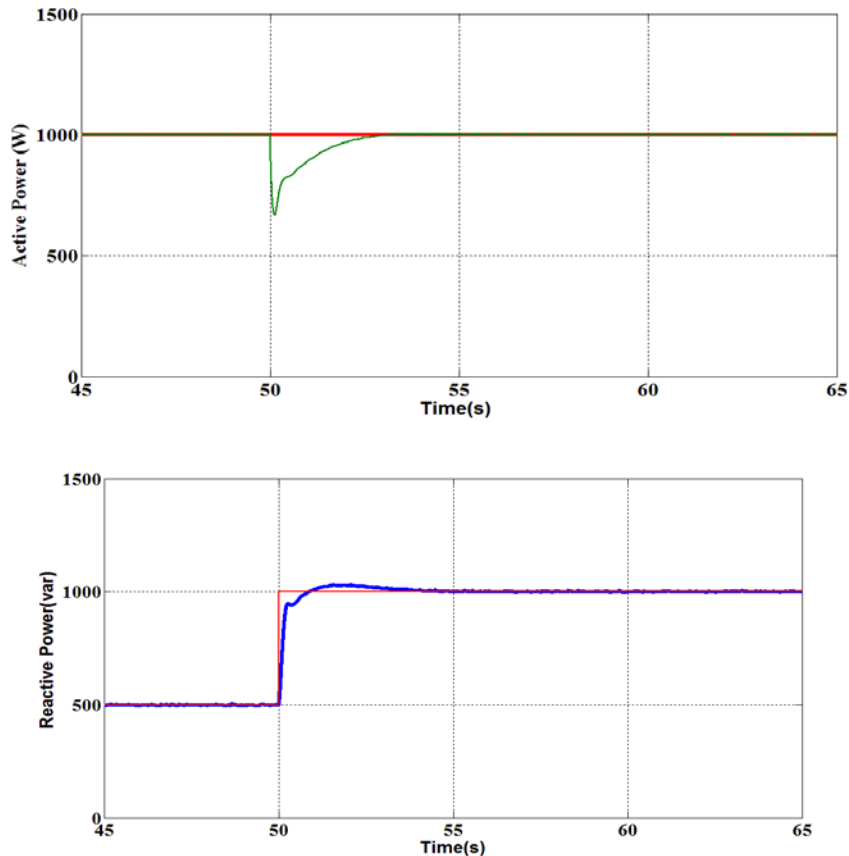

Fig. 5.a) The simulation results of the tracking can be enabled and disabled k_{cp}=20 k_{si}=0.2,,k_{sp}=0.15
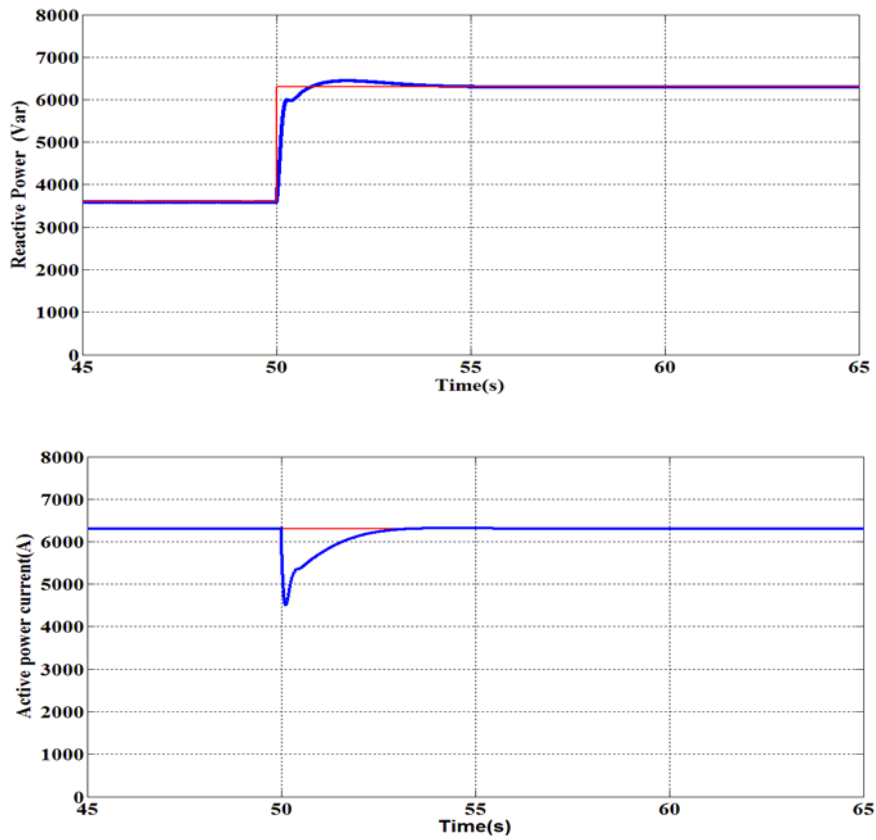
Fig. 5. b) Simulation results of step response tracking can enable and disable the inverter connected to the network k_{cp}=20 , k_{si}=0.2,,k_{sp}=0.15
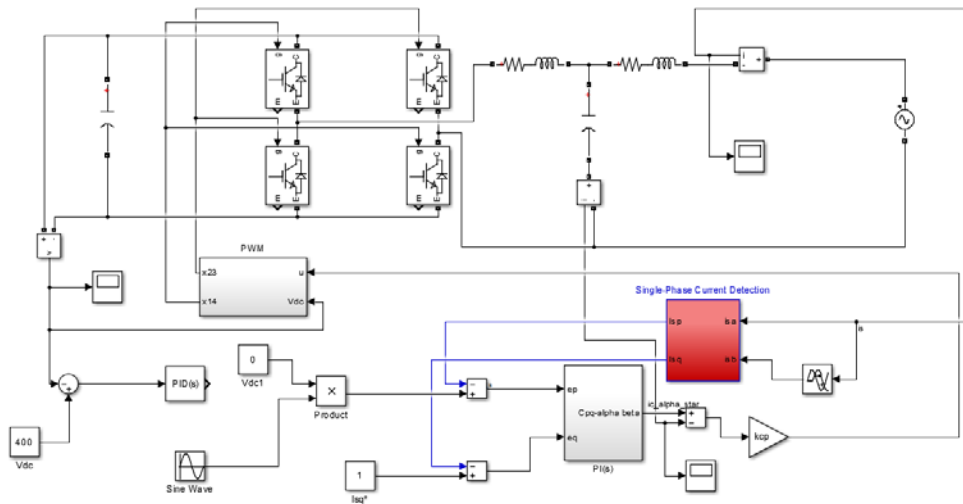

Fig .6. Diagram of the control two-loop simulation

Table 4 .PARAMETER VALUES OF APF CIRCUIT FOR EXPERIMENTAL TEST

|	Parameter	Value
(1)	Grid voltage	110 v-60 htz
(2)	Nominal power	600 VA
(3)	Filter inductance	5 mA
(4)	Filter parasitic resistance	0.34Ω
(5)	Filter capacitor	1.5 mF
(6)	Load parameters	4Ω,45Ω,500 mF
(7)	Nominal load current	4 A
(8)	Nominal first harmonic load current	3.2 A 60 Hz
(9)	V_c RC low-pass filter	90Hz
(10)	PI voltage control	4.5 A/V s, 0.64 A/V,200 V
(11)	K_1u Second-order band-pass filter	60 Hz, 7 Hz
(12)	Maximum switching frequency	18 KHz
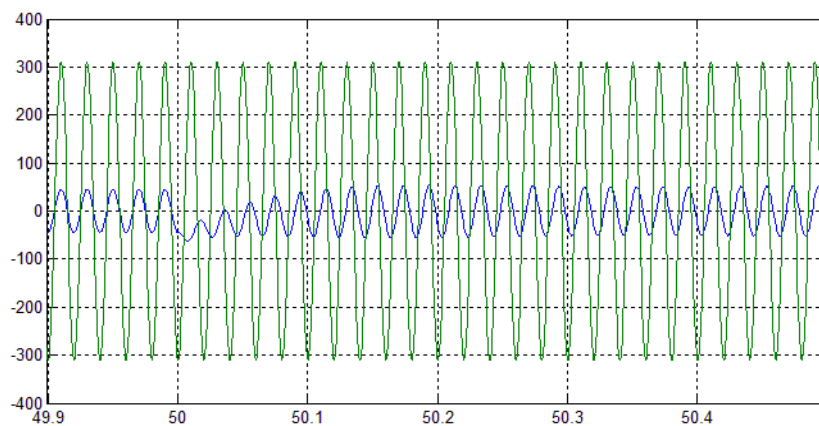
Fig. 7. Simulation results related to the national grid voltage waveform and the current network $k_{cp}=20$,$k_{si}=0.2$, $k_{sp}=0.15$
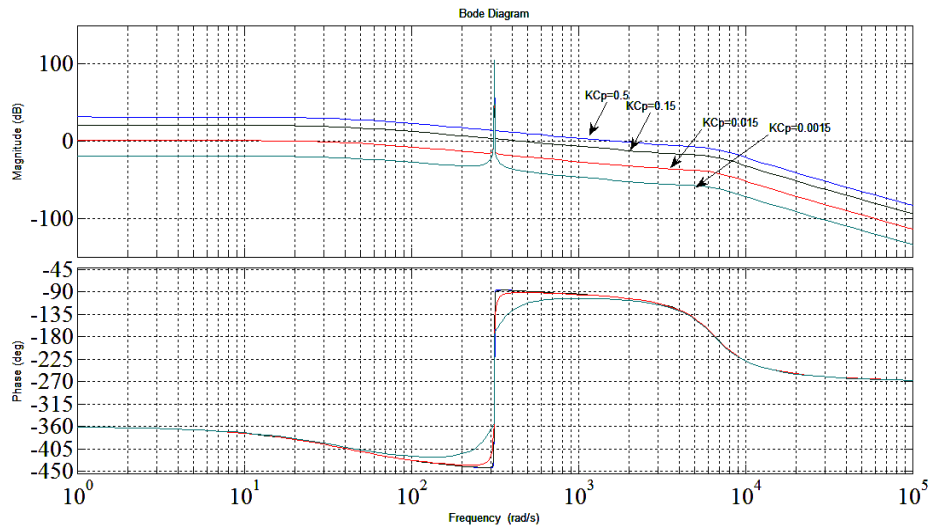
Fig. 8 .Diagram the open loop transfer function for proportional gain inner loop
k_{cp}=20, k_{si}=0.2, k_{sp}=0.15

6-Conclusion

In this article, double-loop control strategy is analyzed in single-phase grid-connected converters. Control system design proposal with regard to the details of the design are studied. The impact on the control system stability with the root locus of the system is analyzed. The outer proportional loop plays an important role on system stability. Increase of the proportional inner loop can eliminate the resonance. Verification of the proposed approach is confirmed by simulation. Reference of the Active and reactive power of the grid connected inverter can be set separately. The ability to understand the multi-functional converter grid-connected renewable energy sources is completely useful. In such a way the reactive power and power factor correction and the ability to single-phase evaluation micro grid operator happen. Suggestion:

To complete this study it can be suggested to consider the following points in future research:

1. Use modern closed-loop controllers and nonlinear regulators instead of linear one

2. Determine the active and reactive power needed in the control loop online and proportional to the load changes

References

[1] J. M. Carrasco, L. G. Franquelo, J. T. Bialasiewicz, E. Galvan, R.C. P. Guisado, M. A. M. Prats, J. I. Leon, and N. Moreno-Alfonso, (2006). "Power electronic for the grid integration of renewable energy sources: a survey," IEEE Transactions on Industrial Electronics, Vol. 53, No. 4, pp. 1002- 1006.

[2] A. A. Ferreira, J. A. Pomilio, G. Spiazzi, and L. de Araujo Silva, (2008). "Energy management fuzzy logic supervisory for electric vehicle power supplies system," IEEE Transactions on Power Electronics, Vol. 23, No. 1, pp. 107-115.

[3] E. Twining and D. G. Holmes, (2003). "Grid current regulation of a three-phase voltage source inverter with an LCL input filter," IEEE Trans. Power Electron., Vol. 18, No. 3, pp. 888-895.

[4] P. C. Loh and D. G. Holmes, (2005). "Analysis of multiloop control strategies for LC/CL/LCL-filtered voltage-source and current-source inverters," IEEE Trans. Ind. Electron., Vol. 41, No. 2, pp. 644-654, Mar.

[5] J. Dannehl, F. W. Fuchs, and P. B. Thøgersen, (2010). "PI state space current control of grid-connected PWM converters with LCL filters," IEEE Trans. Power Electron., Vol. 25, No. 9, pp. 2320-2330.

[6] Liserre M., Blaabjerg F., Hansen S., (2005). "Design and Control of an LCL-Filter-Based Three-Phase Active Rectifier," IEEE Trans. Ind. Appl., vol. 41, no. 5, pp. 1281-1291.

[7] Aslain Ovono Zue and Ambrish Chandra, (2006). "Simulation and Stability Analysis of a 100kW Grid Connected LCL Photovoltaic Inverter for Industry," Power Engineering scociety general meeting 2006, pp.2239-2244.

[8] M. Liserre, A. Dell'Aquila, and F. Blaabjerg, (2004). "Genetic algorithm-based design of the active damping for an LCL-filter three-phase active rectifier," IEEE Trans. Power Electronics, vol. 19, no. 1, pp. 76-86.

[9] M. Liserre, R. Teodorescu, and F. Blaabjerg, (2006). "Stability of Photovoltaic and Wind Turbine Grid-Connected Inverters for a Large Set of Grid Impedance Values," IEEE Transactions on Power Electronics, vol. 21, no.1, pp. 263- 272.

[10] M. Liserre, A. Dell'Aquila, and F. Blaabjerg, (2002). "Stability improvement of an LCL-filter based three-phase active rectifier," PESC'02, vol. 3, pp. 1195-1201.

[11] Leonardo Augusto Serpa, Srinivas Ponnaluri, Peter Mantovanelli Barbosa and Johann Walter Kolar, (2007). "A Modified Direct Power Control Strategy Allowing the Connection of Three-Phase Inverters to the Grid Through LCL Filters," IEEE Trans. Ind. Appl., vol.43, no. 5, pp. 1388-1400.

[12] Guoqiao Shen, Dehong Xu, Danji Xi, Xiaoming Yuan, (2006). "An Improved Control Strategy for Grid-connected Voltage Source Inverters with a LCL Filter," APEC'06, pp. 1067-1073.

[13] Remus Teodorescu, Frede Blaabjerg, Marco Liserre and Antonio Dell'Aquila, (2003). "A stable three-phase LCL-filter based active rectifier without damping," IAS'03, vol. 3, pp. 1552-1557.

[14] E. Twining and D.G. Holmes, (2003). "Grid Current Regulation of a Three-Phase Voltage Source Inverter with an LCL Input Filter," IEEE Trans. Power Electronics, vol. 18, no. 3, pp. 888-895.

[15] L. Mihalache, (2005). "A high performance DSP controller for three-phase PWM rectifiers with ultra low input current THD under unbalanced and distorted input voltage," IAS'05, vol. 1, pp. 138-144.

[16] A. Papavasiliou, S.A. Papathanassiou, S.N. Manias and G. Demetriadis, (2007). "Current Control of a Voltage Source Inverter Connected to the Grid via LCL Filter," PESC'07, pp. 2379-2384.

[17] F.A. Magueed and J. Svensson, (2005). "Control of VSC connected to the grid through LCL-filter to achieve balanced currents," IAS'05, vol. 1, pp. 572-578.

[18] E. Wu and P.W. Lehn, (2006). "Digital current control of a voltage source converter with active damping of LCL resonance," IEEE Trans. Power Electronics, vol. 21, no. 5, pp. 1364- 1373.

[19] Fei Liu, Shanxu Duan, Pengwei Xu, Guoqiang Chen and Fangrui Liu, (2007). "Design and Control of Three-Phase PV Grid Connected

Converter with LCL Filter," IECON'07, pp. 1656-1661.

[20] C. Y. Hsu and H. Y. Wu, (1996). "A new single-phase active power filter with reduced energy-storage capacity," Proc. Inst. Elect. Eng.—Elect. Power Appl., vol. 143, no. 1, pp. 25–30.

[21] K. Mahabir, G. Verghese, J. Thottuvelil, and A. Heyman, (1990). "Linear averaged and sampled data models for large signal control of high power factor AC–DC converters," in Proc. IEEE PESC, pp. 372–381.

[22] R. Ridley, (1989). "Average small-signal analysis of the boost power factor correction circuit," in Proc. Virginia Power Electron. Center Semin., Blacksburg, VA, pp. 108–120.